REVIEW ARTICLE
https://doi.org/10.1038/s41567-018-0062-7
nature physics
Corrected: Publisher Correction

Spin transport and spin torque in antiferromagnetic devices

J. Železný[1,2*], P. Wadley[3], K. Olejník[2], A. Hoffmann[4] and H. Ohno[5,6,7,8]

Ferromagnets are key materials for sensing and memory applications. In contrast, antiferromagnets, which represent the more common form of magnetically ordered materials, have found less practical application beyond their use for establishing reference magnetic orientations via exchange bias. This might change in the future due to the recent progress in materials research and discoveries of antiferromagnetic spintronic phenomena suitable for device applications. Experimental demonstration of the electrical switching and detection of the Néel order open a route towards memory devices based on antiferromagnets. Apart from the radiation and magnetic-field hardness, memory cells fabricated from antiferromagnets can be inherently multilevel, which could be used for neuromorphic computing. Switching speeds attainable in antiferromagnets far exceed those of ferromagnetic and semiconductor memory technologies. Here, we review the recent progress in electronic spin-transport and spin-torque phenomena in antiferromagnets that are dominantly of the relativistic quantum-mechanical origin. We discuss their utility in pure antiferromagnetic or hybrid ferromagnetic/antiferromagnetic memory devices.

Magnetism and technology have been inextricably linked for centuries—from the navigation compass, to motors and generators, to magnetic data storage. The field of information storage has been dominated by ferromagnetic materials from its inception to the present day. Memories based on ferromagnets, such as magnetic tapes and hard disk drives, have been one of the key factors that enabled the information revolution. Antiferromagnetism, on the other hand, has played fleeting roles in the story of information technology so far, despite the fact that antiferromagnetic order is common in magnetic materials. Most of these roles have been as passive elements, such as for pinning or hardening of ferromagnet layers.

The main obstacle that has kept antiferromagnets away from application is that they are hard to control and hard to read. While ferromagnetic order can be detected by the magnetic fields it creates, and in turn manipulated by an external magnetic field, antiferromagnets produce no fringing magnetic fields and are much less sensitive to them (although they can also be manipulated by large enough magnetic fields). So while antiferromagnets could be used for memories, just like ferromagnets, the difficulty of detecting and manipulating the antiferromagnetic order provided a seemingly insurmountable barrier.

While magnetic fields provide a practical way for detecting and manipulating ferromagnetic order, many other methods have been developed. Perhaps most importantly, electrical currents can now be used both for detection and switching of ferromagnetic order. Utilizing electrical currents instead of magnetic fields is more efficient and more scalable, and thus the latest magnetic random access memories rely entirely on electrical currents[1]. The possibility of using electrical currents instead of magnetic fields for detection and manipulation has inspired a renewed interest in antiferromagnetic materials. Electrical manipulation combined with electrical detection of antiferromagnetic order has been recently demonstrated[2]. This shows that antiferromagnets could be used to store information in electronic memory devices and opens new avenues for fundamental research of antiferromagnetic order and dynamics.

Here, we review recent theoretical and experimental progress on spin-transport and spin-torque phenomena allowing for reading and writing information stored in antiferromagnets. See Fig. 1 for a summary of all proposed electrical reading and writing methods. We also discuss other transport phenomena relevant to spintronics such as the generation of spin currents by antiferromagnets due to the spin Hall effect (SHE)[3,4].

Non-relativistic spintronics effects

As discussed in Box 1, antiferromagnetic spintronics initially focused on antiferromagnetic analogues of ferromagnetic spin valves and tunnelling junctions. These devices were theoretically proposed to have the same functionality as their ferromagnetic counterparts, but were found to be strongly sensitive to disorder and perfect epitaxy, which prevented their experimental realization.

A more promising approach might be to consider devices that combine antiferromagnets with ferromagnets, where the ferromagnet functions as a spin polarizer. Gomonay and Loktev[5] showed that a spin-polarized current can efficiently manipulate the antiferromagnetic order, assuming that the torque generated by the spin-polarized current has the same form on each sublattice as is common in ferromagnets, that is, $\mathbf{T}_j \sim \mathbf{M}_j \times (\mathbf{M}_j \times \mathbf{p})$ (the so-called antidamping-like torque). Here j is a sublattice index, $\mathbf{M}_j$ is the magnetic moment on a sublattice j, and $\mathbf{p}$ is the direction of the spin polarization of the current. This form of the torque was subsequently derived in a more rigorous fashion[6,7]. It is instructive to consider why such a torque is effective for manipulating antiferromagnets. The torque can be thought of as being generated by an effective magnetic field, such that $\mathbf{T}_j \sim \mathbf{M}_j \times \mathbf{B}_j$ with $\mathbf{B}_j = \mathbf{M}_j \times \mathbf{p}$. In a collinear antiferromagnet such a field is staggered, that is, alternating in sign between sublattices. It is a general principle that staggered fields can efficiently manipulate antiferromagnets, whereas uniform fields (such as an external magnetic field) cannot. Unlike the spin-transfer torque generated by an antiferromagnet, the torque due to the spin-polarized current is expected to be much more robust against disorder. We refer to the Perspective on

[1]Max Planck Institute for Chemical Physics of Solids, Dresden, Germany. [2]Institute of Physics, Academy of Sciences of the Czech Republic, Praha, Czech Republic. [3]School of Physics and Astronomy, University of Nottingham, Nottingham, UK. [4]Materials Science Division, Argonne National Laboratory, Argonne, IL, USA. [5]Center for Spintronics Integrated Systems, Tohoku University, Sendai, Japan. [6]Center for Innovative Integrated Electronic Systems, Tohoku University, Sendai, Japan. [7]Laboratory for Nanoelectronics and Spintronics, Research Institute of Electrical Communication, Tohoku University, Sendai, Japan. [8]WPI Advanced Institute for Materials Research, Tohoku University, Sendai, Japan. These authors contributed equally: J. Železný and P. Wadley *e-mail: jakub.zelezny@gmail.com

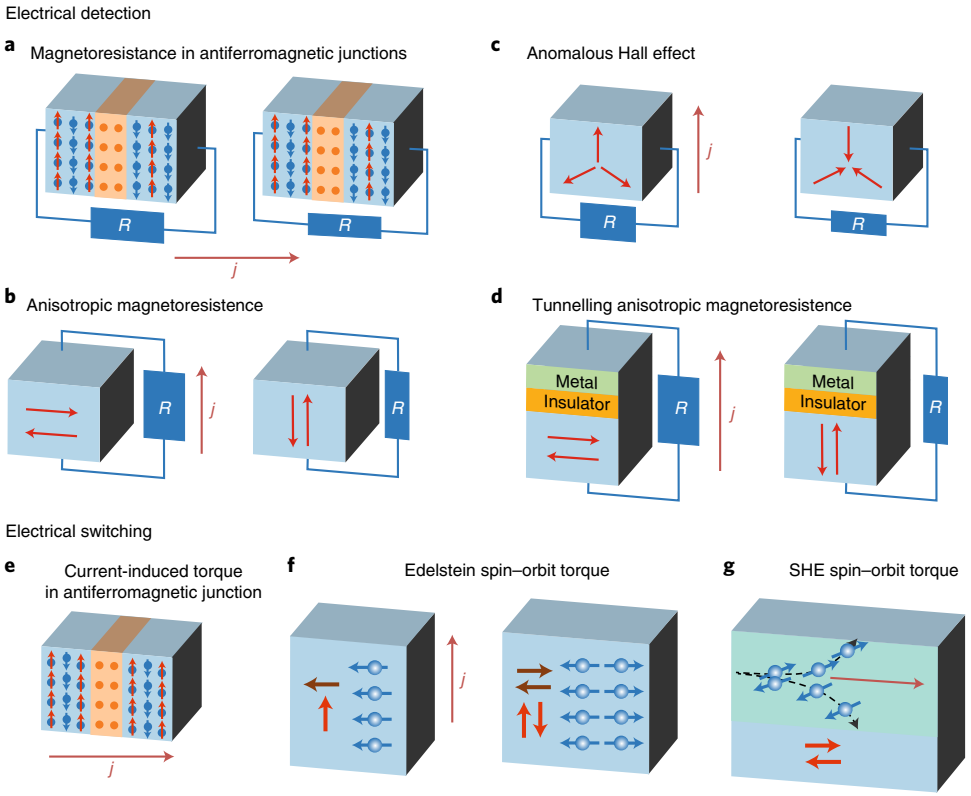

Fig. 1 | Illustration of the various concepts proposed for the electrical detection and manipulation of antiferromagnetic order. In all panels, blue denotes antiferromagnetic or ferromagnetic regions, red arrows denote magnetic moment, *j* denotes electrical current and *R* denotes resistance. **a**, Magnetoresistance in antiferromagnetic spin valve or tunnelling junction. It has been theoretically proposed, but so far has not been clearly detected experimentally. The orange region denotes non-magnetic or insulating spacer. The blue and red arrows denote magnetic moments on the two sublattices. **b**, Anisotropic magnetoresistance. This method has been demonstrated experimentally in several antiferromagnets. **c**, Anomalous Hall effect. This method has been demonstrated experimentally in non-collinear antiferromagnets. **d**, Tunnelling anisotropic magnetoresistance. A large readout signal has been experimentally demonstrated. **e**, Spin-transfer torque in an antiferromagnetic spin valve or tunnelling junction. Such torques were theoretically proposed, but so far have not been demonstrated experimentally. **f**, ISGE spin-orbit torque in a ferromagnet (left) and antiferromagnet (right). The blue arrows illustrate the spin-polarization induced by current. The red and brown arrows denote the initial and final orientations of the magnetic moments. Switching using this torque has been demonstrated experimentally. **g**, The SHE spin-orbit torque. The green region corresponds to a non-magnetic metal, which generates the SHE. The pink arrow denotes the electrical current and the black arrows show the direction of flow for electrons with opposite spin-polarizations (denoted by blue). The torque in such a device has been experimentally demonstrated and switching has been recently observed with insulating antiferromagnets.

dynamics[8] in this Focus issue for more details on the phenomenology of the time-dependent phenomena induced by the staggered fields.

The torques acting on an antiferromagnet due to injection of a spin-polarized current have been studied in ferromagnet/antiferromagnet bilayers in which the ferromagnet and the antiferromagnet are exchange coupled. The exchange coupling leads to a shift of the ferromagnetic hysteresis loop, which is known as exchange bias[9]. Several experiments have observed that electrical current influences the exchange bias[10–15]. This provides indirect evidence that a spin-polarized current can influence antiferromagnets. However, the exact origin of the observed effect is not clear since exchange bias is a complex and not completely understood phenomenon.

The effects we have discussed so far are non-relativistic in origin. In contrast, many of the effects that we will discuss in the following sections are caused by the spin–orbit coupling. This is a relativistic term in the Hamiltonian, which couples the spin and the orbital degree of freedom of an electron. Its significance lies in particular in the fact that it couples spin to the lattice and in this way it lowers the symmetry of the system and can generate a variety of non-equilibrium spin phenomena.

Anisotropic magnetoresistance

The first, and still widely employed, method for electrically detecting a reorientation of the magnetization in a ferromagnet is by using anisotropic magnetoresistance (AMR)[16]: the dependence of the resistance on the direction of the magnetization with respect to current or crystal axes.

AMR tends to be smaller than giant or tunnelling magnetoresistance, however, it is simpler to detect experimentally since it is a bulk effect and thus does not require complex multilayers. Furthermore, as it is an even function of magnetization, it is equally present in antiferromagnetic materials[17]. However, until recently, the effect had remained elusive because of the difficulty in controlling the magnetic moment direction in antiferromagnets. Nevertheless, AMR has now been demonstrated in several antiferromagnets. Marti et al.[18] used antiferromagnetic FeRh for the demonstration of AMR. This material becomes ferromagnetic when heated and responds to applied magnetic fields. By then cooling back into the antiferromagnetic phase with the field still applied, the antiferromagnetic spin direction can be controlled. Other experiments used antiferromagnets exchange coupled to a ferromagnet[19,20], large magnetic fields[21,22] or electrical current[2] (as we discuss in depth later) to manipulate the antiferromagnetic moments. The full functional form of AMR, shown in Fig. 2a, was demonstrated by Kriegner et al.[22] in antiferromagnetic MnTe.

AMR has both longitudinal and symmetric transverse components. Historically, the transverse AMR is sometimes called the planar Hall effect, but we avoid this terminology because the true Hall effects correspond to the antisymmetric off-diagonal

Box 1 | Antiferromagnetic spin valves and tunnelling junctions

Giant[77,78] and tunnelling magnetoresistance[79,80] and spin-transfer torques[81–83] are among the key spintronics phenomena for applications in ferromagnetic memories. These effects occur in devices composed of two ferromagnetic layers separated by a thin metallic or insulating layer (panel a). The metallic devices are called spin valves, while the tunnelling ones are referred to as magnetic tunnelling junctions. Giant and tunnelling magnetoresistance are, respectively, the dependence of the ohmic or tunnel current on the relative magnetization orientations of the two ferromagnetic layers. When an electrical current is flowing through the structure it transfers spin from one layer to the other, which generates a spin-transfer torque. For a sufficiently strong current, this torque enables switching between parallel and antiparallel configurations of the magnetic layers. The spin-transfer torque together with tunnelling magnetoresistance are used to create the basic building blocks of magnetic random access memories[1].

Initial theoretical research in antiferromagnetic spintronics focused on antiferromagnetic analogues of spin valves and tunnelling junctions (see Fig. 1a for illustration of two different states of such junctions). Núñez et al.[84] predicted that in an antiferromagnetic spin valve, a giant magnetoresistance as well as a spin-transfer torque will occur. They illustrated the existence of magnetoresistance and spin-transfer torque with a 1D model (panel b). Subsequent work found that these effects persist in more chemically realistic antiferromagnetic spin-valve structures[85–87] (panel c) and in tunnelling junctions[88,89]. (See also reviews by MacDonald et al.[90] and Haney et al.[91] on the early calculations and comparison to ferromagnets.) Haney et al.[92] have shown that an antiferromagnet can also generate a torque on a ferromagnet. Similarly to ferromagnets, a spin-transfer torque is also predicted to occur for an antiferromagnetic domain wall[86,93,94]. All of these investigations, however, considered ballistic transport in perfectly epitaxial and commensurate heterostructures. A key issue is whether these effects will survive in realistic devices. Duine et al.[95] found that presence of inelastic scattering strongly reduces giant magnetoresistance and the torque, in contrast to ferromagnetic spin valves. Nevertheless, it was argued that magnetoresistance and the torque should survive since the inelastic mean free path is typically relatively large and elastic scattering was assumed to not influence the magnetoresistance and the torque much. However, later studies[87,96,97] found that the torque is very strongly suppressed even by elastic scattering (panel d). Thus the torque (and likely also magnetoresistance) in antiferromagnetic spin valves is probably limited to very clean samples and low temperatures. Recent calculations by Saidaoui et al.[98] suggest that the torque might be more robust against elastic scattering in tunnelling junctions.

A very good epitaxy is expected to be necessary for the presence of magnetoresistance and torque in antiferromagnetic heterostructures. Therefore, while theoretical works have clearly demonstrated that giant and tunnelling magnetoresistances and spin-transfer torques can in principle exist in purely antiferromagnetic structures, the observation of these effects would require clean and perfectly epitaxial devices. This is consistent with the fact that no torque, and only a tiny magnetoresistance[99–101] have been observed in antiferromagnetic spin valves and tunnelling junctions so far.

Finally, we note that the research we have discussed so far focused mostly on collinear antiferromagnets. Recently, Železný et al.[102] predicted that in non-collinear antiferromagnets, such as Mn_3Ir and Mn_3Sn, the electrical current is spin polarized. Thus, a robust torque and magnetoresistance could exist in spin valves or tunnelling junctions based on these antiferromagnets.

Spin valves and tunnelling junctions. a, The two states of a ferromagnetic spin valve or tunnelling junction. **b**, 1D tight-binding model used by Duine et al.[95]. PM denotes non-magnetic (paramagnetic) region, and n_1 and n_2 denote the order parameters of the left and right antiferromagnet. **c**, Chemically realistic antiferromagnetic tunnelling junctions considered by Stamenova et al.[89]. **d**, Calculations by Saidaoui et al.[96] for various spin valves, which show strong decrease of the torque in the presence of elastic scattering in the antiferromagnetic spin valves compared with a ferromagnetic one. Here, λ is the mean free path, L is the length of the spin valve, L_0 correspond to 20 atomic sites and the inset shows normalized conductivities. 'G-type' and 'layered' corresponds to different types of antiferromagnetic spin valve. Reproduced from ref. [95], APS (**b**); ref. [89], APS (**c**); and ref. [96], APS (**d**).

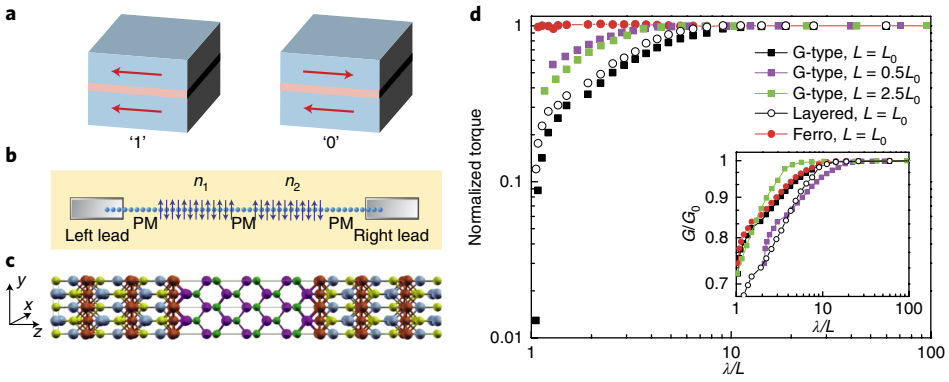

components of the conductivity tensor. Among those, the anomalous Hall effect can also be used for detecting the magnetization reversal in ferromagnets. Unlike AMR, the anomalous Hall effect is an odd function of magnetization and thus not present in collinear antiferromagnets. It has, however, been demonstrated in non-collinear antiferromagnets[23–26] (Fig. 1c). We refer to the article on topological phenomena in this Focus issue for more in-depth discussion of this phenomenon.

AMR is useful for experimental detection of switching of antiferromagnets, however, its small magnitude limits the possible miniaturization and the readout speed in devices[16]. Significantly larger effects can be achieved by using a current tunnelling from an antiferromagnet to a non-magnetic metal, an effect called tunnelling anisotropic magnetoresistance (TAMR) (Fig. 1d). In antiferromagnets, TAMR was predicted by Schick et al.[17] and subsequently demonstrated experimentally by Park et al.[27] who found a very large

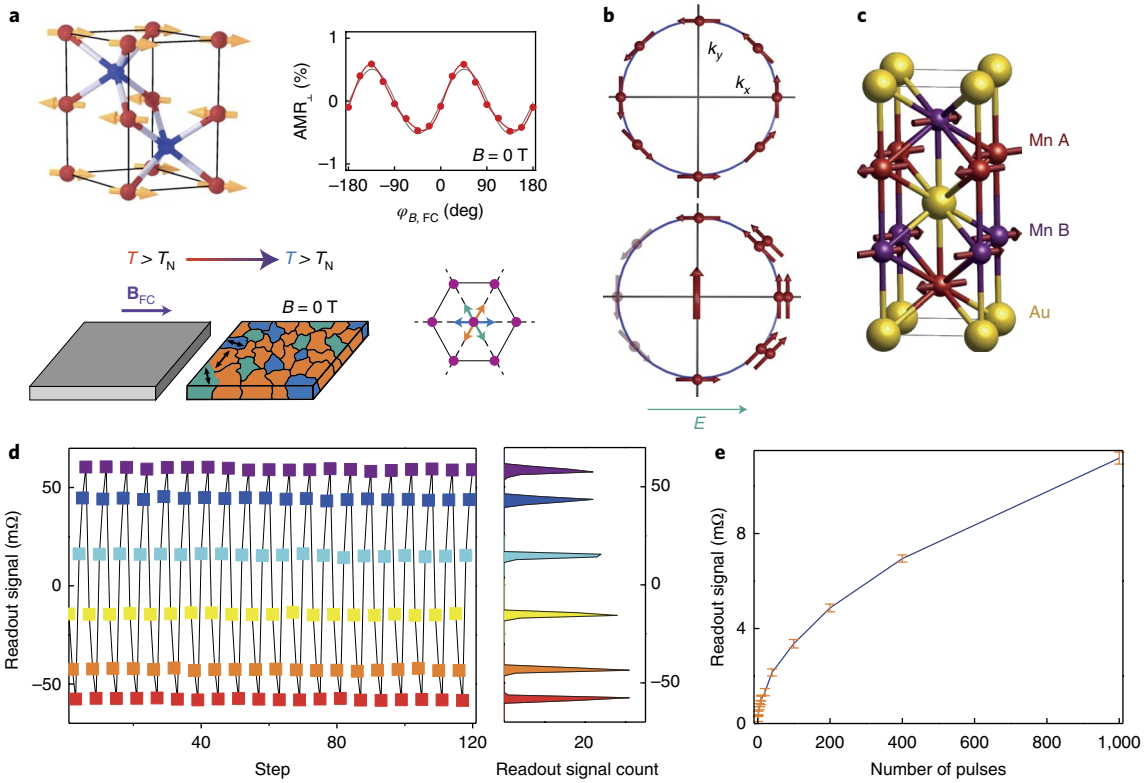

Fig. 2 | AMR and ISGE spin–orbit torque in antiferromagnets. a, Measurement of AMR in MnTe. Top left: the crystal and magnetic structure of MnTe. Top right: the AMR signal obtained by field cooling in magnetic fields with various directions ($\varphi_{B,FC}$). The measurement is done in zero magnetic field (B). Bottom: illustration of the field-cooling procedure. First the sample is heated above the Néel temperature (T_N) and a magnetic field ($\mathbf{B}_{FC}$) is applied. The sample is then cooled below the Néel temperature with the field still present, which results in a distribution of magnetic domains between the three magnetic easy axes (bottom right). **b**, Illustration of the ISGE effect. Top: Fermi surface of a system with spin–orbit coupling in equilibrium, k_x and k_y denote the components of the **k** vector. Bottom: applied electric field (E) causes a redistribution of electrons that results in a non-equilibrium spin polarization. **c**, Crystal and magnetic structure of Mn_2Au. **d**, Left: electrical switching by the ISGE spin–orbit torque in CuMnAs demonstrating the multilevel stability and reproducibility of the results. For the measurement, a series of three 100-μs-long pulses was repeatedly applied along perpendicular directions. Right: histogram of the six different states, obtained from 50 repetitions of the pulse sequence. All measurements were performed at room temperature. **e**, Electrical switching by the ISGE spin–orbit torque in CuMnAs using a series of 250-ps pulses as a function of the number of pulses. The error bars show a standard deviation of 15 repetitions. Adapted from ref. [22], Macmillan Publishers Ltd (**a**); ref. [4], APS (**b**); ref. [42], APS (**c**); and ref. [48], Macmillan Publishers Ltd (**d**,**e**).

TAMR effect in a NiFe/IrMn/MgO/Pt tunnelling junction. The effect can exceed 160% at low temperature. In this work, the NiFe ferromagnetic layer sensitive to weak magnetic fields and exchange coupled with the IrMn antiferromagnet was used to rotate the antiferromagnetic moments to produce different resistance states. The NiFe/IrMn exchange-spring effect was not robust enough to persist to room temperature. Ralph et al.[28] reproduced the large low-temperature TAMR and highlighted a strong sample dependence of the effect whose detailed microscopic description is still missing.

An alternative TAMR structure of [Pt/Co]/IrMn/AlO_x/Pt with a stronger ferromagnet/antiferromagnet exchange coupling used by Wang et al.[29] allowed for the detection of the effect at room temperature. A weak TAMR signal, not exceeding 1% even at low temperatures, was attributed in this structure to the amorphous AlO_x tunnel barrier. Petti et al.[30] demonstrated that the TAMR effect can also exist in structures that contain no ferromagnet using field cooling from above the Néel temperature. More research is needed to understand precisely the TAMR mechanisms and to optimize the structures, however, these experiments demonstrate that a large magnetoresistance can in principle exist in antiferromagnetic structures.

Spin–orbit torque switching

Spin–orbit coupling allows for the generation of a current-induced torque in a magnet without spin injection from an external polarizer. The spin–orbit torque occurs because in crystals with broken inversion symmetry electrical current generates a non-equilibrium spin-polarization (Fig. 2b). This effect is known as the inverse spin-galvanic effect (ISGE) (also called the Edelstein effect)[31–34]. In a magnetic material, the current-induced spin polarization exchange couples to the equilibrium magnetic moments and thus generates a torque. The ISGE spin–orbit torque was theoretically proposed[35–37] and experimentally detected[38,39] in the ferromagnetic semiconductor GaMnAs and recently also in the room-temperature ferromagnetic metal NiMnSb (ref. [40]). For the presence of a net current-induced polarization, the inversion symmetry has to be broken, thus the Edelestein spin–orbit torque can only be used for manipulation of ferromagnets with broken inversion symmetry.

Železný et al.[41,42] predicted that the ISGE spin–orbit torque will also occur in antiferromagnets with appropriate symmetry and that it can efficiently manipulate the antiferromagnetic order. The reason for the efficient manipulation is that with appropriate symmetry the current-induced spin polarization contains a component that is staggered. This staggered component in turn generates a staggered effective magnetic field, which can manipulate the antiferromagnetic order efficiently. Železný et al.[41] calculated the spin–orbit torque for antiferromagnetic Mn_2Au, which has the crystal structure shown in Fig. 2c. The non-magnetic crystal of Mn_2Au has inversion symmetry and, therefore, there is no net current-induced spin polarizations. The Mn sublattices, however, each have locally

broken inversion symmetry. As a consequence, there can be a current-induced spin polarization on each Mn sublattice, but they have to be precisely opposite in the non-magnetic crystal.

The ISGE spin–orbit torque has advantages compared with the other current-induced torques discussed earlier. Because the torque is generated locally, it is not particularly sensitive to disorder[43] and because it is a bulk effect it does not require special heterostructures and thin-film antiferromagnets. On the other hand, it only works in antiferromagnets with the appropriate symmetry. For example, for the presence of the field-like (that is, independent of the magnetic order) ISGE spin–orbit torque, the two spin-sublattices must occupy inversion-partner lattice sites. The switching of an antiferromagnet via this torque was initially demonstrated by Wadley et al.[2] using epilayers of antiferromagnetic CuMnAs that has a symmetry analogous to Mn_2Au. Figure 2d shows a more recent measurement of this switching phenomenon on CuMnAs grown on Si. In CuMnAs (as well as in Mn_2Au), the efficient torque has a field-like character. Because of the symmetry of the crystal, the field is perpendicular to the electrical current[42]. Thus, by applying perpendicular current pulses, the magnetic moments in CuMnAs can be switched between two perpendicular directions. In the experiment by Wadley et al.[2], the switching was monitored by AMR. It was shown that the longitudinal and transverse resistances depend on the direction, amplitude and duration of applied current pulses, in a way that is consistent with the expected ISGE spin–orbit torque. Further experiments used X-ray photoemission electron microscopy, combined with X-ray magnetic linear dichroism, to directly image the antiferromagnetic domain configuration following the current pulses[2,44], confirming the magnetic origin of the electrical signals due to alignment of antiferromagnetic moments orthogonal to the applied current direction. Recently, the spin–orbit torque switching combined with the AMR detection was also confirmed experimentally in sputtered films of Mn_2Au[45,46].

Memory devices

Antiferromagnets possess a number of properties that make them highly favourable for memory applications. Like their ferromagnetic counterparts, their magnetic state is inherently non-volatile, but with the addition that they are robust to external magnetic fields. The antiferromagnetic spin-sublattices with a compensated magnetic moment give them some intriguing additional benefits. The absence of internal dipolar fields favours multistable antiferromagnetic domain configurations, which can be exploited for integrating memory and logic functionality. The antiferromagnetic exchange is also the origin of the ultrafast reorientation dynamics (in the terahertz regime), as well as making antiferromagnets magnetically 'invisible' and enabling denser packing of memory elements.

There have been several demonstrations of antiferromagnetic memory devices based on the concepts we have outlined. The metamagnetic FeRh devices described by Marti et al.[18] demonstrate a memory functionality, where the information bits were represented by perpendicular directions of the antiferromagnetically coupled magnetic moments. Moriyama et al.[47] used the same approach and material system to demonstrate sequential read and write operations of the antiferromagnetic memory stable over a large number of cycles.

The CuMnAs devices described by Wadley et al.[2] demonstrate an antiferromagnetic memory that can be both written (using the spin–orbit torque) and read (using AMR) electrically under ambient conditions (Fig. 3). Olejnik et al.[48] explored the multilevel memory behaviour of these devices further and showed that they could be used to write up to thousands of states (Fig. 2e). By applying successive current pulses, progressively higher reproducible resistance states can be reached depending on the number and duration of the pulses. Both pulse-counting and pulse-time-integration functionalities were demonstrated, for pulse lengths ranging from milliseconds down to 250 ps, close to the limit of contact current injection with commercial pulse generators (Fig. 2e). The micromagnetic domain origins of these multistable states were imaged by Grzybowski et al.[44]. Olejnik et al.[48] also demonstrated the compatibility of CuMnAs memory devices with conventional microelectronic printed circuit boards (Fig. 3c), and low-temperature-growth and fabrication compatibility of CuMnAs with Si or III–V semiconductors (Fig. 3a). These memory devices have a promising potential for applications

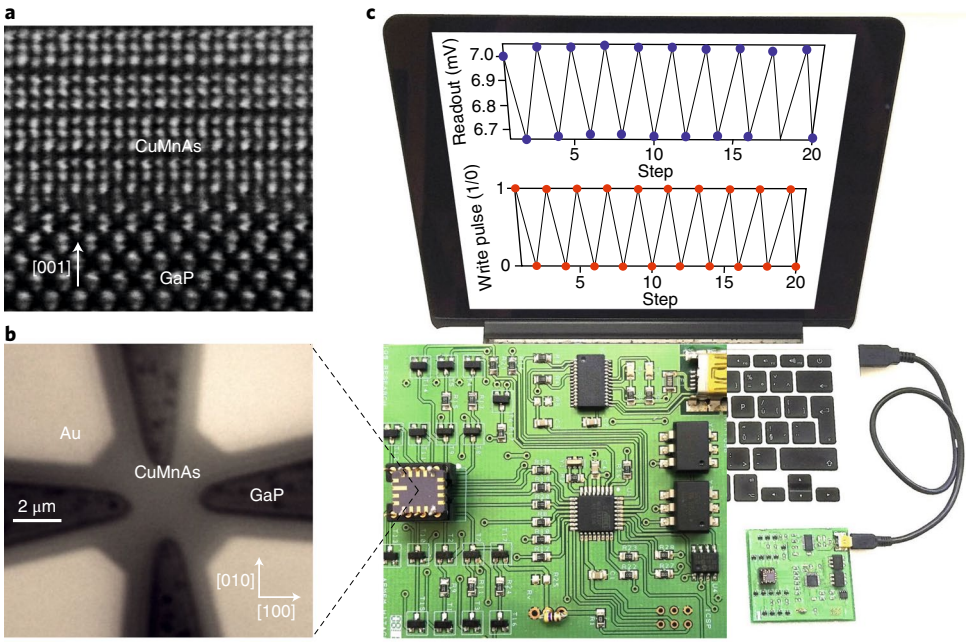

Fig. 3 | Demonstration of microelectronic compatibility of the CuMnAs memory cell. a, Transmission electron miscroscope image of the epitaxial growth of CuMnAs on GaP. **b**, The CuMnAs device used for electrical switching. **c**, The electrical switching of CuMnAs in a USB device. Reproduced from ref. [48], Macmillan Publishers Ltd.

based on their multilevel character, such as neuromorphic computing or pulse counters. The readout signals are, at this point, too small for application as a conventional bistable memory. However, with device and materials optimization and utilizing a different readout method such as TAMR, the readout signals can likely be increased significantly. These memories could then potentially be used as conventional memories in situations where speed is very important, such as the central processing unit (CPU) caches.

Recently, switching by picosecond pulses of terahertz radiation, combined with AMR readout, has been demonstrated in the same CuMnAs bit-cells[49]. The switching in these experiments has a multilevel character, similar to the electrical switching. This shows that a non-contact switching of an antiferromagnet is also feasible and opens a path to the development of antiferromagnetic memories for the terahertz band. In contrast, ferromagnets are limited by the GHz writing speed threshold. For writing speeds up to the GHz scale, weak fields are sufficient for switching ferromagnetic moments and the associated energy cost decreases with increasing speed. Above the GHz threshold, however, the trend reverses, with both the field and the energy cost increasing proportionally to the writing speed[50,51]. As a result, current-induced spin–orbit torque switching has not been pushed in ferromagnetic memory devices to writing speeds exceeding 5 GHz (ref. [51]).

Another intriguing concept for magnetic memory is a memory based on the movement of magnetic domain walls, the so-called racetrack memory. Antiferromagnets are of interest for such memories because antiferromagnetic domain walls were recently predicted to move much faster than ferromagnetic domain walls[52,53]. We refer to the article on dynamics in this Focus issue for detailed discussion of this topic.

In this Review, we have mostly focused on transport phenomena. An exciting possibility is also the control of magnetic order by electric field in magnetic insulators. Such functionality has been demonstrated in magnetoelectric material Cr_2O_3 (ref. [54]) and in multiferroic materials that combine ferroelectricity and antiferromagnetism. See the review article by Sando et al.[55] for a description of recent progress on the most commonly used multiferroic material $BiFeO_3$.

Spin Hall effect in antiferromagnets

When current flows through a material, a spin current appears flowing in a direction transverse to the charge current. This effect is known as the SHE[3,4]. It originates due to the spin–orbit coupling, which causes the electrons with opposite spin to deflect in opposite directions thus creating a spin current. The inverse effect also exists: when a spin current is injected into a material with spin–orbit coupling, a transverse voltage appears. The direct and inverse SHE are of key importance for spintronics since they allow for transforming between charge currents and spin currents.

The SHE can be used to generate a spin–orbit torque, which can switch a ferromagnet[56,57]. When a SHE material is interfaced with a ferromagnet and electrical field is applied parallel to the interface, a spin current flows into the ferromagnet and generates a torque on the magnetization. It allows, in principle, for a faster and more efficient switching of ferromagnetic layers than spin-transfer torque[58]. Note that the SHE mechanism coexists with the ISGE spin–orbit torque since interfaces break the inversion symmetry of the structure[4].

The spin–orbit torque due to the SHE could also be used to manipulate antiferromagnetic moments[41] (Fig. 1g). As discussed above, spin current injected into an antiferromagnet generates a torque that can efficiently manipulate the antiferromagnetic order. Such spin current could be injected from a ferromagnet, but the spin current due to the SHE could also be used. A spin–orbit torque in a heavy-metal/antiferromagnet configuration has indeed been observed experimentally[59]. However, the difficulty of manipulating the antiferromagnetic order by magnetic fields did not allow for a detailed characterization of the torque as is routinely done in heavy-metal/ferromagnet bilayers. Recently, switching of antiferromagnetic NiO, attributed to the SHE spin–orbit torque, has been observed in Pt/NiO/Pt multilayers[60].

In the past, research of the SHE focused mostly on non-magnetic materials. It is, however, allowed by symmetry in any material, including antiferromagnetic (and other magnetic) materials. The SHE has been found theoretically and experimentally in several antiferromagnets[61–63]. Instead of the direct SHE, these experiments demonstrated the inverse SHE, which can be detected electrically by injecting a pure spin current into the antiferromagnet. The spin current is generated by a ferromagnet either using precessing magnetization (the so-called spin pumping), as illustrated in Fig. 4b, or alternatively using a heat gradient. An example of d.c. voltages measured in a spin-pumping experiment for antiferromagnets MnX, X = Fe, Pd, Ir and Pt (Fig. 4a), is given in Fig. 4c. Several of the antiferromagnets showed a large SHE comparable to the commonly used non-magnetic heavy metals. In addition, the spin Hall conductivities along different crystalline axes are highly anisotropic in these antiferromagnetic alloys as has been demonstrated with measurements of epitaxial films with different growth orientations[64]. This behaviour is consistent with intrinsic spin Hall effects as determined by first-principles calculations. Furthermore, the spin Hall conductivity seems to be susceptible to manipulation via different magnetic field and temperature cycles, resulting in different arrangements of the antiferromagnetic spin structure[65].

Since antiferromagnets can have a large SHE, it is expected that they can also be used to generate a spin–orbit torque on a ferromagnet. This has been confirmed by several experiments for various antiferromagnets[59,64–72]. The observed spin–orbit torque can be very large, comparable to the largest values for non-magnetic heavy metals. Switching of ferromagnetic layers by the spin–orbit torque has also been demonstrated[67–69,72]. Using an antiferromagnet instead of a non-magnetic metal has some unique advantages. For the spin–orbit torque switching it is preferable to use a perpendicularly magnetized ferromagnet since this allows for faster switching and better scalability. However, in such a case, a constant in-plane magnetic field has to be applied to achieve deterministic switching[73]. Conversely, an antiferromagnet can be exchanged coupled to the ferromagnet, thus allowing field-free switching[67–69,72]. Another remarkable feature that was observed in antiferromagnet/ferromagnet bilayers[67] is a memristor behaviour (Fig. 4e,f), reminiscent of the multilevel spin–orbit torque switching in bulk antiferromagnets (CuMnAs, Mn_2Au) discussed above[2,45,48]. This behaviour is of great importance for neuromorphic computing where it can simulate synapses. It is attributed to a progressive current-induced switching of more magnetic domains in the ferromagnet, which are then kept fixed by the exchange coupling with the antiferromagnet (Fig. 4d). A proof-of-concept artificial neural network based on the spin–orbit torque in a PtMn/CoNi structure has already been demonstrated[74].

Outlook

The basic memory functionality, including electrical writing and readout has been demonstrated in antiferromagnets. Within a year of the initial demonstration of spin–orbit torque switching, the electrical pulse length has been reduced from milliseconds to picoseconds, opening a prospect of ultra-fast magnetic memories. The Heusler-compound-related CuMnAs antiferromagnet used in the experiments can be grown epitaxially, and devices can be microfabricated on III–V or Si substrates, allowing for future integration in semiconductor circuits. Spin–orbit torque switching has also been demonstrated in Mn_2Au, which broadens the range of suitable materials to sputtered transition-metal films. Multilevel (memristor) switching is commonly observed in memories made of single-layer antiferromagnets or antiferromagnet/ferromagnet bilayers.

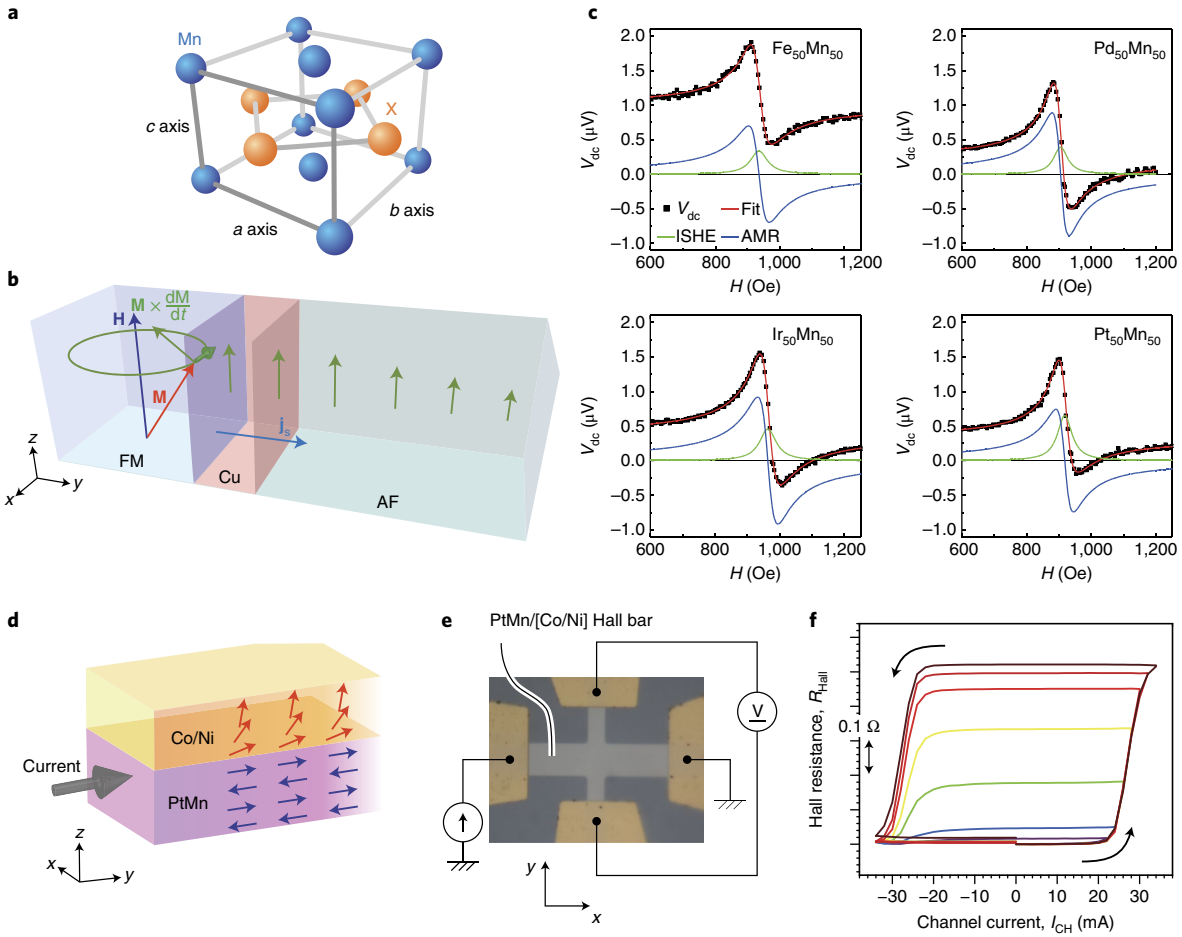

Fig. 4 | The SHE and the SHE spin–orbit torque in antiferromagnets. a, Crystal structure of antiferromagnets MnX. **b**, Schematic of the spin-pumping experiments. Combination of a d.c. and a.c. magnetic field (**H**) induces a precession of the magnetization (**M** denotes the magnetization and d**M**/d*t* is its time derivative) of the ferromagnetic (FM) layer, which causes a spin current ($\mathbf{j}_s$) flowing in the antiferromagnet (AF). The spin current is then converted to voltage due to the inverse SHE. **c**, Voltages detected in the spin-pumping experiment as a function of a d.c. magnetic field for several MnX antiferromagnets. The total signal contains a contribution from the inverse SHE and AMR. **d**, Illustration of the exchange bias in antiferromagnet/ferromagnet bilayers, which leads to a memristor-like behaviour of the spin–orbit torque switching. **e**. The experimental set-up used for the demonstration of the memristor behaviour. **f**, Demonstration of the memristor-like behaviour in the PtMn/[Co/Ni] devices. 0.5-s-long current pulses with magnitude varying between $-I_{max}$ and I_{max} were applied and the Hall resistance was measured after each pulse. Different values of I_{max} are denoted by different colours. Reproduced from ref. [61], APS (**a**–**c**); ref. [67], Macmillan Publishers Ltd (**d**); and ref. [74], IOP (**e**,**f**).

Momentum in the research area of antiferromagnetic spintronics is immense, yet much remains to be done. To fully utilize the potential of antiferromagnets, several key aspects must be better understood. The factors that contribute to the complex domain structures, and their relative importance, need to be elucidated in order to design and engineer devices and material properties with the requisite domain patterns and stability for specific memory applications. The ultra-fast switching needs to be studied in detail. And promising steps have been made towards time-resolved optical detection[75], as discussed in this Focus issue in the Review on opto-spintronics[76].

The electrical readout signals observed in antiferromagnets at room temperature have so far been relatively small. This could be sufficient for some applications, but larger readout signals would be desirable for high-density fast readout memory application. Device and materials optimization is necessary to extend the large readout signals observed at low temperatures to room temperature. The only electrical switching method that has been demonstrated so far is the bulk ISGE spin–orbit torque. Switching using the spin–orbit torque due to the SHE could be more efficient and is expected to work in any antiferromagnet, whereas the ISGE spin–orbit torque requires antiferromagnets with specific symmetry. More materials research is necessary to identify other antiferromagnets that could be switched via the ISGE spin–orbit torque. The spin–orbit torque generated by antiferromagnets on ferromagnets in the antiferromagnet/ferromagnet bilayers is promising, although its origin is not entirely understood. It is commonly attributed to the SHE, but this has not been proven and other effects are likely to contribute. Of particular interest is understanding how the spin–orbit torque and the SHE depend on the antiferromagnetic order.

Received: 30 May 2017; Accepted: 26 January 2018;
Published online: 2 March 2018

References

1. Chappert, C., Fert, A. & Van Dau, F. N. The emergence of spin electronics in data storage. *Nat. Mater.* **6**, 813–823 (2007).
2. Wadley, P. et al. Electrical switching of an antiferromagnet. *Science* **351**, 587–590 (2016).
3. Hoffmann, A. Spin Hall effects in metals. *IEEE Trans. Magn.* **49**, 5172–5193 (2013).
4. Sinova, J., Valenzuela, S. O., Wunderlich, J., Back, C. H. & Jungwirth, T. Spin Hall effects. *Rev. Mod. Phys.* **87**, 1213–1260 (2015).

5. Gomonay, H. V. & Loktev, V. M. Spin transfer and current-induced switching in antiferromagnets. *Phys. Rev. B* **81**, 144427 (2010).
6. Gomonay, H. V., Kunitsyn, R. V. & Loktev, V. M. Symmetry and the macroscopic dynamics of antiferromagnetic materials in the presence of spin-polarized current. *Phys. Rev. B* **85**, 134446 (2012).
7. Cheng, R., Xiao, J., Niu, Q. & Brataas, A. Spin pumping and spin-transfer torques in antiferromagnets. *Phys. Rev. Lett.* **113**, 057601 (2014).
8 Gomonay, O., Baltz, V., Brataas, A. & Tserkovnyak, Y. Antiferromagnetic spin textures and dynamics. *Nat. Phys.* https://doi.org/10.1038/s41567-018-0049-4 (2018).
9. Nogués, J. et al. Exchange bias in nanostructures. *Phys. Rep.* **422**, 65–117 (2005).
10. Wei, Z. et al. Changing exchange bias in spin valves with an electric current. *Phys. Rev. Lett.* **98**, 116603 (2007).
11. Urazhdin, S. & Anthony, N. Effect of polarized current on the magnetic state of an antiferromagnet. *Phys. Rev. Lett.* **99**, 046602 (2007).
12. Wei, Z., Basset, J., Sharma, A., Bass, J. & Tsoi, M. Spin-transfer interactions in exchange-biased spin valves. *J. Appl. Phys.* **105**, 07D108 (2009).
13. Tang, X. L., Zhang, H. W., Su, H., Zhong, Z. Y. & Jing, Y. L. Changing and reversing the exchange bias in a current-in-plane spin valve by means of an electric current. *Appl. Phys. Lett.* **91**, 122504 (2007).
14. Dai, N. V. et al. Impact of in-plane currents on magnetoresistance properties of an exchange-biased spin valve with an insulating antiferromagnetic layer. *Phys. Rev. B* **77**, 132406 (2008).
15. Tang, X., Su, H., Zhang, H. W., Jing, Y. L. & Zhong, Z. Y. Tuning the direction of exchange bias in ferromagnetic/antiferromagnetic bilayer by angular-dependent spin-polarized current. *J. Appl. Phys.* **112**, 073916 (2012).
16. Daughton, J. Magnetoresistive memory technology. *Thin Solid Films* **216**, 162–168 (1992).
17. Shick, A. B., Khmelevskyi, S., Mryasov, O. N., Wunderlich, J. & Jungwirth, T. Spin-orbit coupling induced anisotropy effects in bimetallic antiferromagnets: a route towards antiferromagnetic spintronics. *Phys. Rev. B* **81**, 212409 (2010).
18. Marti, X. et al. Room-temperature antiferromagnetic memory resistor. *Nat. Mater.* **13**, 367–374 (2014).
19. Fina, I. et al. Anisotropic magnetoresistance in an antiferromagnetic semiconductor. *Nat. Commun.* **5**, 4671 (2014).
20. Zhang, X. & Zou, L. K. Planar Hall effect in $Y_3Fe_5O_{12}$/IrMn films. *Appl. Phys. Lett.* **105**, 262401 (2014).
21. Wong, A. T. et al. Strain driven anisotropic magnetoresistance in antiferromagnetic $La_{0.4}Sr_{0.6}MnO_3$. *Appl. Phys. Lett.* **105**, 052401 (2014).
22. Kriegner, D. et al. Multiple-stable anisotropic magnetoresistance memory in antiferromagnetic MnTe. *Nat. Commun.* **7**, 11623 (2016).
23. Chen, H., Niu, Q. & MacDonald, A. H. Anomalous Hall effect arising from noncollinear antiferromagnetism. *Phys. Rev. Lett.* **112**, 017205 (2014).
24. Kübler, J. & Felser, C. Non-collinear antiferromagnets and the anomalous Hall effect. *Europhys. Lett.* **108**, 67001 (2014).
25. Nakatsuji, S., Kiyohara, N. & Higo, T. Large anomalous Hall effect in a non-collinear antiferromagnet at room temperature. *Nature* **527**, 212–215 (2015).
26. Nayak, A. K. et al. Large anomalous Hall effect driven by a nonvanishing Berry curvature in the noncolinear antiferromagnet Mn_3Ge. *Sci. Adv.* **2**, e1501870 (2016).
27. Park, B. G. et al. A spin-valve-like magnetoresistance of an antiferromagnet-based tunnel junction. *Nat. Mater.* **10**, 347–351 (2011).
28. Ralph, D. Spintronics research at Cornell. *UCSB* http://online.kitp.ucsb.edu/online/spintronics13/ralph/ (2013).
29. Wang, Y. Y. et al. Room-temperature perpendicular exchange coupling and tunneling anisotropic magnetoresistance in an antiferromagnet-based tunnel junction. *Phys. Rev. Lett.* **109**, 137201 (2012).
30. Petti, D. et al. Storing magnetic information in IrMn/MgO/Ta tunnel junctions via field-cooling. *Appl. Phys. Lett.* **102**, 192404 (2013).
31. Edelstein, V. M. Spin polarization of conduction electrons induced by electric current in two-dimensional asymmetric electron systems. *Solid State Commun.* **73**, 233–235 (1990).
32. Silov, A. Y. et al. Current-induced spin polarization at a single heterojunction. *Appl. Phys. Lett.* **85**, 5929–5931 (2004).
33. Kato, Y., Myers, R., Gossard, A. & Awschalom, D. Current-induced spin polarization in strained semiconductors. *Phys. Rev. Lett.* **93**, 176601 (2004).
34. Wunderlich, J., Kaestner, B., Sinova, J. & Jungwirth, T. Experimental observation of the spin-Hall effect in a two-dimensional spin-orbit coupled semiconductor system. *Phys. Rev. Lett.* **94**, 047204 (2005).
35. Bernevig, B. A. & Vafek, O. Piezo-magnetoelectric effects in p-doped semiconductors. *Phys. Rev. B* **72**, 033203 (2005).
36. Manchon, A. & Zhang, S. Theory of nonequilibrium intrinsic spin torque in a single nanomagnet. *Phys. Rev. B* **78**, 212405 (2008).
37. Garate, I. & MacDonald, A. H. Influence of a transport current on magnetic anisotropy in gyrotropic ferromagnets. *Phys. Rev. B* **80**, 134403 (2009).
38. Chernyshov, A. et al. Evidence for reversible control of magnetization in a ferromagnetic material by means of spin-orbit magnetic field. *Nat. Phys.* **5**, 656–659 (2009).
39. Fang, D. et al. Spin-orbit-driven ferromagnetic resonance. *Nat. Nanotech.* **6**, 413–417 (2011).
40. Ciccarelli, C. et al. Room-temperature spin–orbit torque in NiMnSb. *Nat. Phys.* **12**, 855–860 (2016).
41. Železný, J. et al. Relativistic Néel-order fields induced by electrical current in antiferromagnets. *Phys. Rev. Lett.* **113**, 157201 (2014).
42. Železný, J. et al. Spin-orbit torques in locally and globally noncentrosymmetric crystals: antiferromagnets and ferromagnets. *Phys. Rev. B* **95**, 014403 (2017).
43. Saidaoui, H. B. M. & Manchon, A. Spin orbit torque in disordered antiferromagnets. Preprint at http://arXiv.org/abs/1606.04261 (2016).
44. Grzybowski, M. J. et al. Imaging current-induced switching of antiferromagnetic domains in CuMnAs. *Phys. Rev. Lett.* **118**, 057701 (2017).
45. Bodnar, S. Y. et al. Writing and reading antiferromagnetic Mn_2Au by Néel spin-orbit torques and large anisotropic magnetoresistance. *Nat. Commun.* **9**, 348 (2018)
46. Meinert, M., Graulich, D. & Matalla-Wagner, T. Key role of thermal activation in the electrical switching of antiferromagnetic Mn2Au. Preprint at http://arXiv.org/abs/1706.06983 (2017).
47. Moriyama, T. et al. Sequential write-read operations in FeRh antiferromagnetic memory. *Appl. Phys. Lett.* **107**, 122403 (2015).
48. Olejník, K. et al. Antiferromagnetic CuMnAs multi-level memory cell with microelectronic compatibility. *Nat. Commun.* **8**, 15434 (2017).
49. Olejník, K. et al. THz electrical writing speed in an antiferromagnetic. Preprint at http://arXiv.org/abs/1711.08444 (2017).
50. Bedau, D. et al. Spin-transfer pulse switching: from the dynamic to the thermally activated regime. *Appl. Phys. Lett.* **97**, 262502 (2010).
51. Garello, K. et al. Ultrafast magnetization switching by spin-orbit torques. *Appl. Phys. Lett.* **105**, 212402 (2014).
52. Gomonay, O., Jungwirth, T. & Sinova, J. High antiferromagnetic domain wall velocity induced by Néel spin-orbit torques. *Phys. Rev. Lett.* **117**, 017202 (2016).
53. Shiino, T. et al. Antiferromagnetic domain wall motion driven by spin-orbit torques. *Phys. Rev. Lett.* **117**, 087203 (2016).
54. Kosub, T. et al. Purely antiferromagnetic magnetoelectric random access memory. *Nat. Commun.* **8**, 13985 (2017).
55. Sando, D., Barthélémy, A. & Bibes, M. $BiFeO_3$ epitaxial thin films and devices: past, present and future. *J. Phys. Condens. Matter* **26**, 473201 (2014).
56. Miron, I. M. et al. Perpendicular switching of a single ferromagnetic layer induced by in-plane current injection. *Nature* **476**, 189–193 (2011).
57. Liu, L. et al. Spin-torque switching with the giant spin Hall effect of tantalum. *Science* **336**, 555–558 (2012).
58. Prenat, G. et al. Ultra-fast and high-reliability SOT-MRAM: from cache replacement to normally-off computing. *IEEE Trans. Multi-Scale Computing Systems* **2**, 49–60 (2016).
59. Reichlová, H. et al. Current induced torques in structures with ultra-thin IrMn antiferromagnet. *Phys. Rev. B* **92**, 165424 (2015).
60. Moriyama, T., Oda, K. & Ono, T. Spin torque control of antiferromagnetic moments in NiO. Preprint at http://arXiv.org/abs/1708.07682 (2017).
61. Zhang, W. et al. Spin Hall effects in metallic antiferromagnets. *Phys. Rev. Lett.* **113**, 196602 (2014).
62. Mendes, J. B. S. et al. Large inverse spin Hall effect in the antiferromagnetic metal $Ir_{20}Mn_{80}$. *Phys. Rev. B* **89**, 140406 (2014).
63. Qu, D., Huang, S. Y. & Chien, C. L. Inverse spin Hall effect in Cr: independence of antiferromagnetic ordering. *Phys. Rev. B* **92**, 020418 (2015).
64. Zhang, W. et al. All-electrical manipulation of magnetization dynamics in a ferromagnet by antiferromagnets with anisotropic spin Hall effects. *Phys. Rev. B* **92**, 144405 (2015).
65. Zhang, W. et al. Giant facet-dependent spin-orbit torque and spin Hall conductivity in the triangular antiferromagnet $IrMn_3$. *Sci. Adv.* **2**, e1600759 (2016).
66. Tshitoyan, V. et al. Electrical manipulation of ferromagnetic NiFe by antiferromagnetic IrMn. *Phys. Rev. B* **92**, 214406 (2015).
67. Fukami, S., Zhang, C., Duttagupta, S., Kurenkov, A. & Ohno, H. Magnetization switching by spin–orbit torque in an antiferromagnet–ferromagnet bilayer system. *Nat. Mater.* **15**, 535–542 (2016).
68. Oh, Y.-W. et al. Field-free switching of perpendicular magnetization through spin–orbit torque in antiferromagnet/ferromagnet/oxide structures. *Nat. Nanotech.* **11**, 878–884 (2016).
69. van den Brink, A. et al. Field-free magnetization reversal by spin-Hall effect and exchange bias. *Nat. Commun.* **7**, 10854 (2016).
70. Wu, D. et al. Spin-orbit torques in perpendicularly magnetized $Ir_{22}Mn_{78}$/$Co_{20}Fe_{60}B_{20}$/MgO multilayer. *Appl. Phys. Lett.* **109**, 222401 (2016).

71. Ou, Y., Shi, S., Ralph, D. C. & Buhrman, R. A. Strong spin Hall effect in the antiferromagnet PtMn. *Phys. Rev. B* **93**, 220405 (2016).
72. Kurenkov, A., Zhang, C., DuttaGupta, S., Fukami, S. & Ohno, H. Device-size dependence of field-free spin-orbit torque induced magnetization switching in antiferromagnet/ferromagnet structures. *Appl. Phys. Lett.* **110**, 092410 (2017).
73. Liu, L., Lee, O. J., Gudmundsen, T. J., Ralph, D. C. & Buhrman, R. A. Current-induced switching of perpendicularly magnetized magnetic layers using spin torque from the spin Hall effect. *Phys. Rev. Lett.* **109**, 096602 (2012).
74. Borders, W. A. et al. Analogue spin–orbit torque device for artificial-neural-network-based associative memory operation. *Appl. Phys. Express* **10**, 013007 (2017).
75. Saidl, V. et al. Optical determination of the Néel vector in a CuMnAs thin-film antiferromagnet. *Nat. Photon.* **11**, 91–96 (2017).
76 Němec, P., Fiebig, M., Kampfrath, T. & Kimel, A. V. Antiferromagnetic opto-spintronics. *Nat. Phys.* https://doi.org/10.1038/s41567-018-0051-x (2018).
77. Baibich, M. N. et al. Giant Magnetoresistance of (001)Fe/(001)Cr Magnetic Superlattices. *Phys. Rev. Lett.* **61**, 2472–2475 (1988).
78. Binasch, G., Grünberg, P., Saurenbach, F. & Zinn, W. Enhanced magnetoresistance in layered magnetic structures with antiferromagnetic interlayer exchange. *Phys. Rev. B* **39**, 4828–4830 (1989).
79. Miyazaki, T. & Tezuka, N. Giant magnetic tunneling effect in Fe/Al_2O_3/Fe junction. *J. Magn. Magn. Mater.* **139**, L231–L234 (1995).
80. Moodera, J. S., Kinder, L. R., Wong, T. M. & Meservey, R. Large magnetoresistance at room temperature in ferromagnetic thin film tunnel junctions. *Phys. Rev. Lett.* **74**, 3273–3276 (1995).
81. Slonczewski, J. C. Conductance and exchange coupling of two ferromagnets separated by a tunneling barrier. *Phys. Rev. B* **39**, 6995–7002 (1989).
82. Berger, L. Emission of spin waves by a magnetic multilayer traversed by a current. *Phys. Rev. B* **54**, 9353–9358 (1996).
83. Ralph, D. C. & Stiles, M. D. Spin transfer torques. *J. Magn. Magn. Mater.* **320**, 1190–1216 (2008).
84. Núñez, A. S., Duine, R. A., Haney, P. M. & MacDonald, A. Theory of spin torques and giant magnetoresistance in antiferromagnetic metals. *Phys. Rev. B* **73**, 214426 (2006).
85. Haney, P. M. et al. Ab initio giant magnetoresistance and current-induced torques in Cr/Au/Cr multilayers. *Phys. Rev. B* **75**, 174428 (2007).
86. Xu, Y., Wang, S. & Xia, K. Spin-transfer torques in antiferromagnetic metals from first principles. *Phys. Rev. Lett.* **100**, 226602 (2008).
87. Prakhya, K., Popescu, A. & Haney, P. M. Current-induced torques between ferromagnets and compensated antiferromagnets: symmetry and phase coherence effects. *Phys. Rev. B* **89**, 054421 (2014).
88. Merodio, P., Kalitsov, A., Béa, H., Baltz, V. & Chshiev, M. Spin-dependent transport in antiferromagnetic tunnel junctions. *Appl. Phys. Lett.* **105**, 122403 (2014).
89. Stamenova, M., Mohebbi, R., Seyed-Yazdi, J., Rungger, I. & Sanvito, S. First-principles spin-transfer torque in CuMnAs|GaP|CuMnAs junctions. *Phys. Rev. B* **95**, 060403 (2017).
90. MacDonald, A. H. & Tsoi, M. Antiferromagnetic metal spintronics. *Phil. Trans. R. Soc. A* **369**, 3098–3114 (2011).
91. Haney, P. M., Duine, R. A., Núñez, A. S. & MacDonald, A. H. Current-induced torques in magnetic metals: beyond spin-transfer. *J. Magn. Magn. Mater.* **320**, 1300–1311 (2008).
92. Haney, P. M. & MacDonald, A. H. Current-induced torques due to compensated antiferromagnets. *Phys. Rev. Lett.* **100**, 196801 (2008).
93. Hals, K. M. D., Tserkovnyak, Y. & Brataas, A. Phenomenology of current-induced dynamics in antiferromagnets. *Phys. Rev. Lett.* **106**, 107206 (2011).
94. Yamane, Y., Ieda, J. & Sinova, J. Spin-transfer torques in antiferromagnetic textures: efficiency and quantification method. *Phys. Rev. B* **94**, 054409 (2016).
95. Duine, R. A., Haney, P. M., Núñez, A. S. & MacDonald, A. Inelastic scattering in ferromagnetic and antiferromagnetic spin valves. *Phys. Rev. B* **75**, 014433 (2007).
96. Saidaoui, H. B. M., Manchon, A. & Waintal, X. Spin transfer torque in antiferromagnetic spin valves: from clean to disordered regimes. *Phys. Rev. B* **89**, 174430 (2014).
97. Manchon, A. Spin diffusion and torques in disordered antiferromagnets. *J. Phys. Condens. Matter* **29**, 104002 (2017).
98. Saidaoui, H., Manchon, A. & Waintal, X. Robust spin transfer torque in antiferromagnetic tunnel junctions. *Phys. Rev. B* **95**, 134424 (2017).
99. Wang, L., Wang, S. G., Rizwan, S., Qin, Q. H. & Han, X. F. Magnetoresistance effect in antiferromagnet/nonmagnet/antiferromagnet multilayers. *Appl. Phys. Lett.* **95**, 152512 (2009).
100. Wei, Z., Sharma, A., Bass, J. & Tsoi, M. Point-contact search for antiferromagnetic giant magnetoresistance. *J. Appl. Phys.* **105**, 07D113 (2009).
101. Wang, Y. et al. Anti-ferromagnet controlled tunneling magnetoresistance. *Adv. Funct. Mater.* **24**, 6806–6810 (2014).
102. Železný, J., Zhang, Y., Felser, C. & Yan, B. Spin-polarized current in non-collinear antiferromagnets. *Phys. Rev. Lett.* **119**, 187204 (2017).

Acknowledgements

We acknowledge support from EU FET Open RIA grant no. 766566. The contributions from A.H. preparing this manuscript were supported by the Department of Energy, Office of Science, Materials Science and Engineering Division. J.Ž. acknowledges support from the Institute of Physics of the Czech Academy of Sciences and the Max Planck Society through the Max Planck Partner Group programme. P.W. acknowledges support from Engineering and Physical Sciences Research Council grant EP/P019749/1 and from the Royal Society through a University Research Fellowship.

Competing interests

The authors declare no competing interests.

Additional information

Reprints and permissions information is available at www.nature.com/reprints.

Correspondence and requests for materials should be addressed to J.Ž.

Publisher's note: Springer Nature remains neutral with regard to jurisdictional claims in published maps and institutional affiliations.